Effect of nanoparticles shape on turbulent nanofluids flow within a solar collector by using hexagonal cross-section tubes

Yacine Khetib [a,b], Hala M. Abo-Dief [c], Abdullah K. Alanazi [c], S. Mohammad Sajadi [d,e], Rasool Kalbasi [f,*], Mohsen Sharifpur [g,h,*]

[a] Mechanical Engineering Department, Faculty of Engineering, King Abdulaziz University, Jeddah 80204, Saudi Arabia
[b] Center Excellence of Renewable Energy and Power, King Abdulaziz University, Jeddah 80204, Saudi Arabia
[c] Department of Chemistry, College of Science, Taif University, P.O. Box 11099, Taif 21944, Saudi Arabia
[d] Department of Nutrition, Cihan University-Erbil, Kurdistan Region, Iraq
[e] Department of Phytochemistry, SRC, Soran University, KRG, Iraq
[f] Independent Researcher
[g] Department of Mechanical and Aeronautical Engineering, University of Pretoria, Pretoria 0002, South Africa
[h] Department of Medical Research, China Medical University Hospital, China Medical University, Taichung 404, Taiwan

ARTICLE INFO

Keywords:
Flat plate solar collector
Nanoparticle shape
Turbulence

ABSTRACT

This paper investigates the turbulent flow of nanofluid (NFs) in which boehmite-alumina nanoparticles with different shapes of platelet, brick, blade, and cylinder suspended in a mixture of W/EG in a flat plate solar collector (FPSC). A hexagonal cross-sectional tube is used in the FPSC and compared with a simple one. The problem variables include flow rate (FR) (0.25–1 kg / s), shape and volume percentage (φ) of nanoparticles (NPs) (0–4%), tube shape (circular and hexagonal) and FPSC material (copper and steel). The influence of these variables on the FPSC output temperature (TC_{OUT}), Nusselt number (Nu) and heat transfer coefficient (h) is investigated. The results reveal that copper FPSC can provide higher TC_{OUT} but has lower convective coeffient and Nu than steel FPSC. The outlet fluid temperature is 1.86 °C higher when pure fluid flows in copper tubes. The addition of NPs, particularly bricks, causes the temperature of the fluid at the outlet to rise. This increase is about 1°for φ = 4%. The use of a hexagonal tube enhances the temperature of the fluid at the outlet relative to a circular one. For copper and steel FPSCs, this increase is 2.67 and 1.75 °C for pure fluid, respectively. The addition of NPs reduces the amount of heat transfer and Nu for the FPSCs.

Introduction

The fact that one day fossil fuels will run out on the one hand and the Earth's climate changes on the other hand has led different countries around the world to find new sources of energy for themselves [1]. Energy issues are of great interest to researchers today [2–6]. Human need for energy is inevitable and reliable energy supply is needed to maintain human comfort. Researchers have also presented various articles in this field [7–10]. Researchers in some of these articles have been looking for a suitable solution to reduce energy consumption of various devices. With regard to environmental issues, however, some researchers have sought different solutions to extract energy from natural and clean sources such as wind energy, sea waves, geothermal and etc. These energy sources are free and do not contain environmental pollution from fossil fuels. They are also endless resources and are renewable. Meanwhile, solar energy as a source for future human energy has been considered by many researchers [11,12]. The enormous source of this energy and its infinity on the one hand, and its easy extraction and availability in most parts of the earth on the other hand, has caused many developed countries in the world to invest in this energy [13,14]. Flat plate solar collectors (FPSCs) have always been one of the solar devices that researchers have always considered due to their comfortable construction and ability to make hot water required for home use [15–17]. These collectors are typically made by placing a tube on an absorbent plate. So far, many researchers have studied FPSCs [18–20]. Most of these researches have been looking for a solution to increase the thermal efficiency of the collector and have tried to increase the temperature of the fluid leaving the collector [21,22]. Sharafaldin and Grof

* Corresponding authors at: Department of Mechanical and Aeronautical Engineering, University of Pretoria, Pretoria 0002, South Africa (M. Sharifpur).
E-mail addresses: rasool.kalbasi@gmail.com (R. Kalbasi), mohsen.sharifpur@up.ac.za (M. Sharifpur).

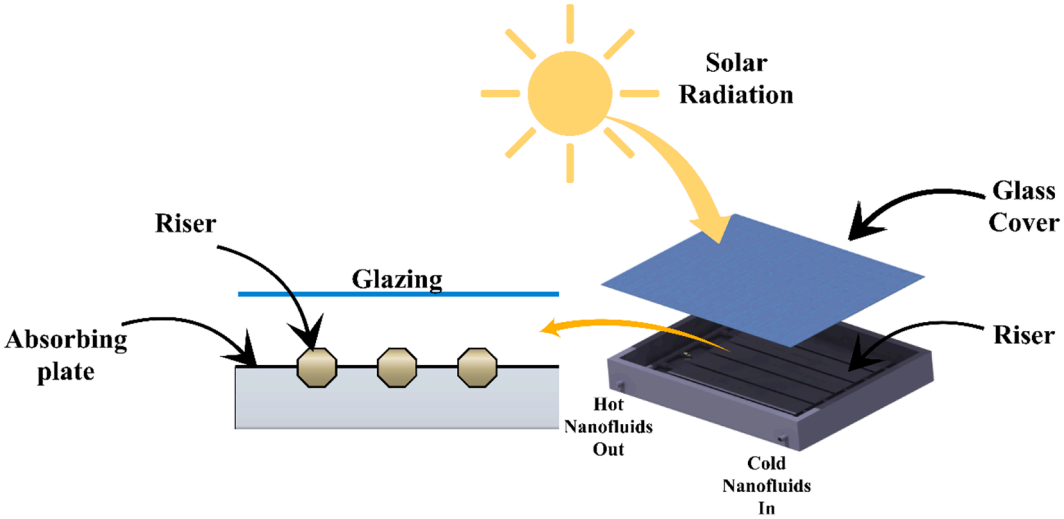

Fig. 1. Schematic of the FPSC.

[23] in a study investigated the effect of flow rate on the efficiency of a FPSC. They used a parallel plate collector for their work. Their findings showed that increasing the flow rate increases the collector efficiency. Laboratory methods for research have been used by many researchers due to their high accuracy and reliability. But because of the high cost as well as the time-consuming, it has also maked problems for researchers. Therefore, researchers have used different numerical methods for their articles [24–28].

Nanotechnology is used in a wide range of engineering devices today [29,30]. In recent decades, researchers have used nanofluids (NFs) in heat exchangers [31–33], chambers [34,35], solar panels [36,37], etc. NFs are composed of one or more metallic or non-metallic nanoparticles (NPs) in liquids such as water, ethylene glycol, etc. [38,39]. This mixture has better thermal conductivity and at the same time higher viscosity in most cases than its base fluid [40–43]. Therefore, researchers have sought to find the right volume percentage of nanoparticles so that they can have the highest heat transfer at the lowest pressure drop. One of the applications of NFs is in solar collectors [44,45]. Many researchers have

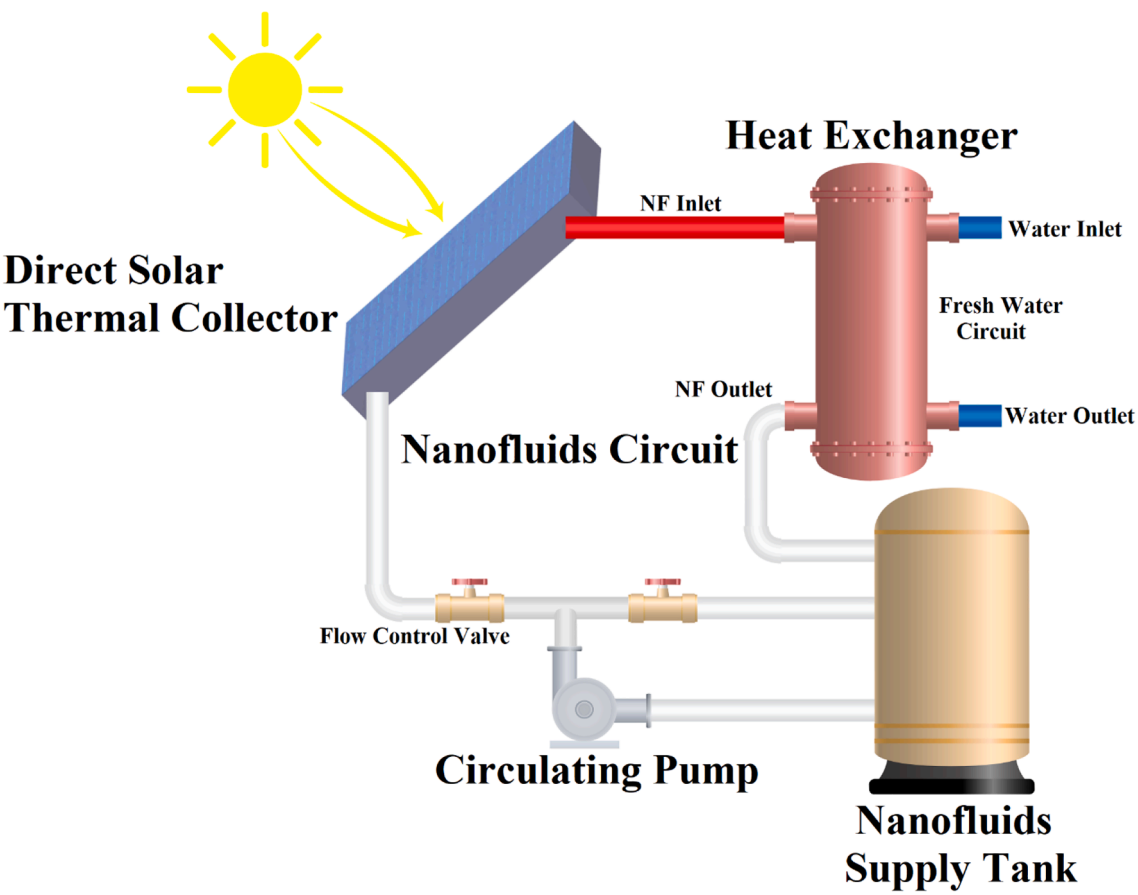

Fig. 2. Schematic of how to use the FPSC in the solar cycle.

used solar collectors containing different NFs and measured its effect. [39,46] Among these, some researchers have investigated the effect of using NFs containing NPs with different shapes in different heating devices. In one of these studies, Yan et al. [47] investigated the effect of using different NPs on heat transfer. They found that the use of NPs with different shapes has an important effect on heat transfer. Dehaj and Mohiabadi [44] investigated the efficiency of a solar collector in a laboratory research. They used MgO-water NF as the working fluid of the system. They studied the effect of mass flow rate and volume percentage of NPs on solar collector efficiency and found that increasing the flow rate improves thermal performance. The addition of NPs also increased the thermal performance of the collector compared to the working fluid state of water alone. Also, increasing the volume percentage increased the performance.

The number of solar energy consumers in the world is increasing every day. The safety and cleanliness of this energy is one of the important characteristics of increasing the use of this energy. FPSCs are one of the types of solar devices that are used for solar water heaters in many homes. Due to the importance of thermal efficiency in collectors, in this paper, a FPSCs with the presence of NF containing NPs with different shapes in different flow rate is investigated. Hexagonal pipes have been used to make the collector. For fabrication also two materials of steel and copper have been used to make pipes and absorbent plate. The values of Nusselt number (Nu) for both collector materials have been compared with each other. Finally, by changing the mass flow rate of NF and its volume percentage for different shapes of NPs, the Nu, heat transfer coefficient and temperature of the fluid leaving the collector have been studied. The innovation of the present work can be summarized in the study of NF turbulence flow in the collector with two types of pipes with two different materials.

Problem description

As shown in Fig. 1, the geometry includes a FPSC with hexagonal tubes. The NFs flow with boehmite-alumina NPs suspended in ethylene glycol/water (50/50) flows in the FPSC tubes. A schematic of the geometry is also given in Fig. 1. The dimensions of the studied collector are 99.8 cm by 48.6 cm. The pipes are placed in parallel in the collector as shown in Fig. 1.

FPSCs are made of copper or steel. The thermal conductivity of copper is 401 and steel is 43 W/mK. Their relative roughness values are 0.0004 and 0.006, respectively. Fig. 2 shows how to use the FPSC in the solar cycle.

Governing equations

The governing equations of a homogeneous Newtonian and incompressible NFs turbulent flow are expressed as follows using the k-ω SST model [48]. Gravity and viscosity loss are also neglected.

$$\frac{\partial(\rho u_j)}{\partial x_j} = 0 \tag{1}$$

$$\frac{\partial}{\partial x_j}(\rho u_i u_j) = -\frac{\partial p}{\partial x_i} + \frac{\partial}{\partial x_j}\left[\mu\left(\frac{\partial u_i}{\partial x_j} + \frac{\partial u_j}{\partial x_i}\right)\right] - \frac{2}{3}\mu\frac{\partial u_i}{\partial x_j}\delta_{ij} + \frac{\partial}{\partial x_j}\left(-\rho\overline{u_i' u_j'}\right) \tag{2}$$

$$\frac{\partial}{\partial x_j}(\rho u_j C_p T) = \frac{\partial}{\partial x_i}\left(k_{nf}\frac{\partial T}{\partial x_i}\right) \tag{3}$$

where C_p is the specific heat capacity of the fluid, T is the fluid temperature, ρ is the density, p is the fluid pressure, x_j is the Cartesian vector coordinate, u_j is the partial velocity, μ is the dynamic viscosity, and δ_{ij} is the Cranker delta.

Based on the conventional k-ω model [50], Menter [49] created the k-ω SST turbulence model. This model may be used to simulate turbulent flow with a low Reynolds number [51–54]. Zhang and Che [55] studied various turbulence models for winding tubes and ducts and found that the best model that is consistent with the experimental results is the k-ω SST the Reynolds number is not too large. Therefore, in this article, this model is used. Its equations are as follows:

$$\frac{\partial}{\partial x_j}(\rho u_j k) = p - 0.09\rho\omega k + \frac{\partial}{\partial x_j}\left[(\mu + \sigma_k\mu_t)\frac{\partial k}{\partial x_j}\right] \tag{4}$$

$$\frac{\partial}{\partial x_j}(\rho u_j \omega) = \frac{\gamma\omega}{k}p - \alpha\rho\omega^2 + \frac{\partial}{\partial x_j}\left[(\mu + \sigma_\omega\mu_t)\frac{\partial\omega}{\partial x_j}\right] + 2(1+F_1)\frac{0.865\rho}{\omega}\frac{\partial k}{\partial x_j}\frac{\partial\omega}{\partial x_j} \tag{5}$$

where [56]:

$$\alpha = 0.075F_1 + 0.0828(1-F_1) \tag{6}$$

$$\gamma = 0.553F_1 + 0.44(1-F_1)$$

$$\sigma_k = 0.5F_1 + (1-F_1)$$

$$\sigma_\omega = 0.5F_1 + 0.865(1-F_1)$$

The values of p and F_1 are also defined as follows [56]:

$$p = \mu_t\left(2\Omega_{ij} - \frac{2}{3}\frac{\partial u_k}{\partial x_k}\delta_{ij}\right) - \frac{2}{3}\rho k\delta_{ij} \tag{7}$$

$$F_1 = tanh^4\left\{min\left[max\left(\frac{\sqrt{k}}{0.09\omega y}; \frac{500\rho\mu}{y^2\omega}\right)\right]\right\}; \frac{3.46\rho k}{CD_{k\omega}y^2} \tag{8}$$

$CD_{k\omega}$ is:

$$CD_{k\omega} = max\left(\frac{1.73\rho}{\omega}\frac{\partial k}{\partial x_j}\frac{\partial\omega}{\partial x_j}; 10^{-20}\right) \tag{9}$$

Eddy viscosity is also obtained from the following equation [56]:

$$\mu_t = \frac{0.31\rho k}{max(0.31\omega; \Omega F_2)} \tag{10}$$

where $\Omega = \sqrt{2\Omega_{ij}\Omega_{ij}}$ is the vorticity [57]. The values of F_2 and Ω_{ij} are:

$$F_2 = tanh^2\left\{max\left(\frac{2\sqrt{k}}{0.09\omega y}; \frac{500\rho\mu}{y^2\omega}\right)\right\} \tag{11}$$

$$\Omega_{ij} = \frac{1}{2}\left(\frac{\partial u_i}{\partial x_j} - \frac{\partial u_j}{\partial x_i}\right) \tag{12}$$

where y is the distance from the current surface to the next [56]. The following is the definition of h and Nu [56]:

$$h = \frac{q''_{ave}}{T_{s,ave} - T_{b,ave}} \tag{13}$$

$$Nu = \frac{hl}{k_{nf}} \tag{14}$$

l is the tube's hydraulic diameter, and k denotes the NFs' thermal conductivity.

NFs properties

The properties of boehmite- alumina/water-EG NFs are discussed [58]:

$$\rho_{nf} = \varphi\rho_{AlOOH} + (1-\varphi)\rho_{W-EG} \tag{15}$$

$$c_{p,nf} = \frac{(1-\varphi)(\rho c_p)_{W-EG} + \varphi(\rho c_p)_{AlOOH}}{\rho_{nf}} \tag{16}$$

$$\frac{\mu n_f}{\mu_{W-EG}} = 1 + A_1\varphi + A_2\varphi^2 \tag{17}$$

Table 1
Constants for different shapes of nanoparticle [58].

	C_k	A_1	A_2
Platelets	2.61	37.1	612.6
Blades	2.74	14.6	123.3
Cylinders	3.95	13.5	904.4
Bricks	3.37	1.9	471.4

Table 2
Thermophysical properties of NPs and base fluid [58].

Property	C_P(J/kg.K)	k(W/m.K)	ρ(kg/m^3)	μ(kg/m.s)
Water/EG	3300	0.3799	1067.5	0.00339
AlOOH	618.3	30	3050	–

$$\frac{kn_f}{k_{W-EG}} = 1 + C_k\varphi \tag{18}$$

The values of constants are given in Table 1.

Table 2 lists the characteristics of the base fluid and NPs, and Fig. 3 depicts a schematic of NP form.

Boundary conditions

Homogeneous and Newtonian NFs enters the FPSC tube at a constant velocity and exits at a constant pressure. The relative output pressure of the FPSC is 0 Pa. A constant heat flux of 500 W/m^2 is applied to the FPSC by solar radiation. The no-slip boundary condition is imposed on the walls.

Numerical method, grid study, and validation

Numerical methods have a wide range of applicants from microfluidic [59,60] to nanofluid and even solar systems to reduce the cost of experiments. The volume control approach is used to solve the NFs turbulence flow equations. The equations are linearized using the second-order method, and the equations are coupled using the SIMPLE algorithm. Finally, boundary conditions are used to model the geometry using ANSYS FLUENT software. The problem is modelled using the energy equation, the turbulence equation, and solar radiation. The approximate time of each solution performed according to the mesh with a home system including CPU i7 6meg cash and 8DDR4 RAM was between 80 and 100 min.

The influence of the number of elements on the outcomes is investigated using various simulations. When the FR is 0.25 kg/s, Table 3 shows the influence of the number of components on the water outlet temperature. The reference grid can be chosen from 3.8 million components based on the results of Table 3. The number of elements has been rounded and stated.

The results of this article are compared to the results of other relevant articles in order to assess the simulations' accuracy. One of these comparisons is done with the article published by Saffarian et al. [61]. This article simulates 3 types of solar FPSCs. In this regard, the Nu is compared with the reference paper [61] (Table 4), indicating low values of error percentage between the two works. The highest error between the present work and the reviewed article was 2.3%.

Results and discussion

Fig. 4 demonstrates NFs TC_{OUT} with different shapes of NPs for different values of φ when the FR is 0.25 kg/s for the copper FPSC. It can

Table 3
The influence of the number of components on the water outlet temperature at a FR of 0.25 kg/s for both tube types.

Number of elements (million)	1.5	2.7	3.2	3.8	4.3
Cu	311.2	309.6	308.8	308.2	308.2
St	310.5	308.5	307.1	306.3	306.3

Table 4
Nu variations for different Reynolds numbers obtained from the present work and Ref. [61].

Re	2500	5000	10,000	15,000	18,000
Ref. [59]	24.41	47.67	94.18	130.23	165.11
This work	24.28	47.16	92.58	127.11	162.58
Error	0.5%	1.0%	1.6%	2.3%	1.5%

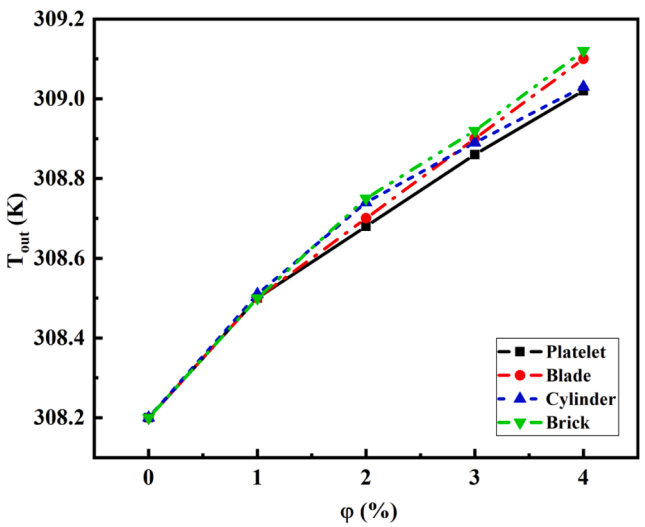

Fig. 4. NFs TC_{OUT} with different shapes of NPs for different values of φ when the FR is 0.25 kg/s for the copper FPSC.

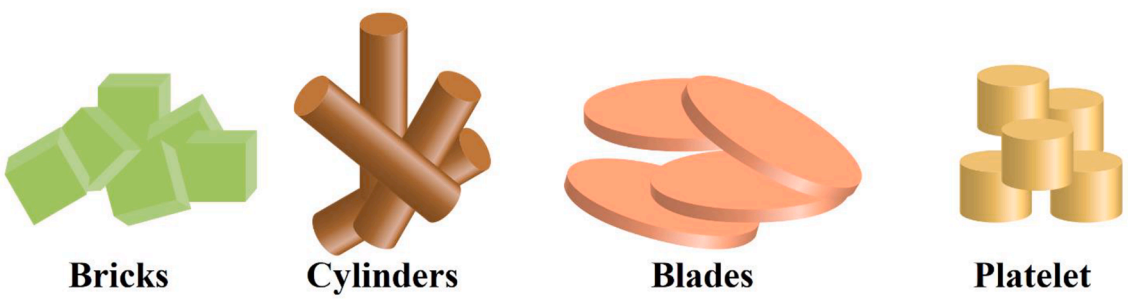

Fig. 3. Schematic of the shape of NPs.

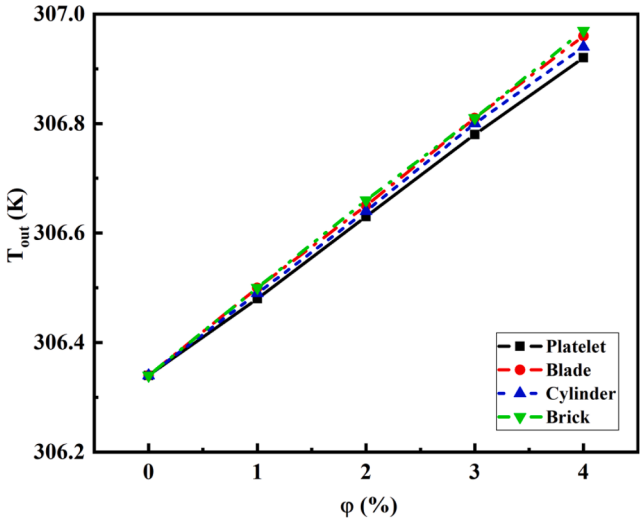

Fig. 5. NFs TC_{OUT} with different shapes of NPs for different values of φ when the FR is 0.25 kg/s for steel FPSC.

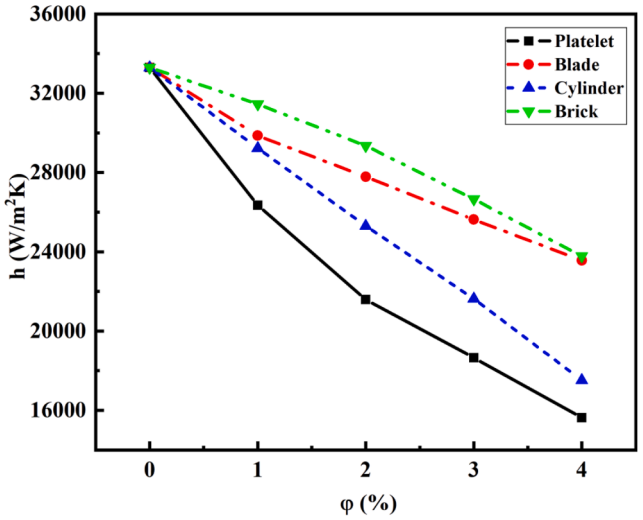

Fig. 7. FPSC h for NFs s with different nanoparticle shapes, different values of φ at a FR of 0.25 kg/s in the copper FPSC.

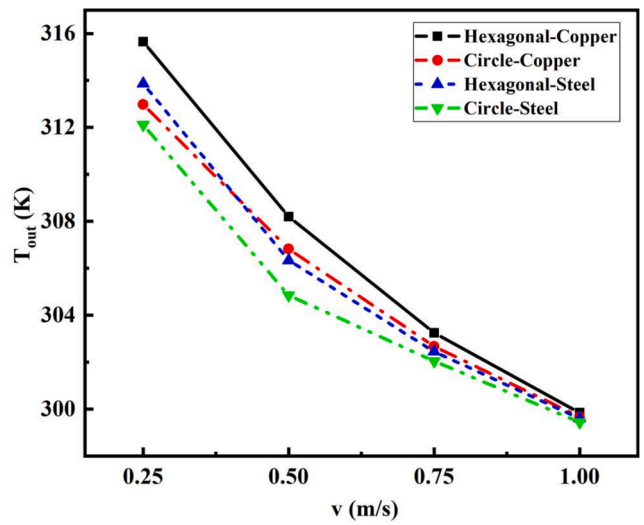

Fig. 6. Water-EG outlet temperature for different FR s in copper and steel FPSCs with circular and hexagonal tubes.

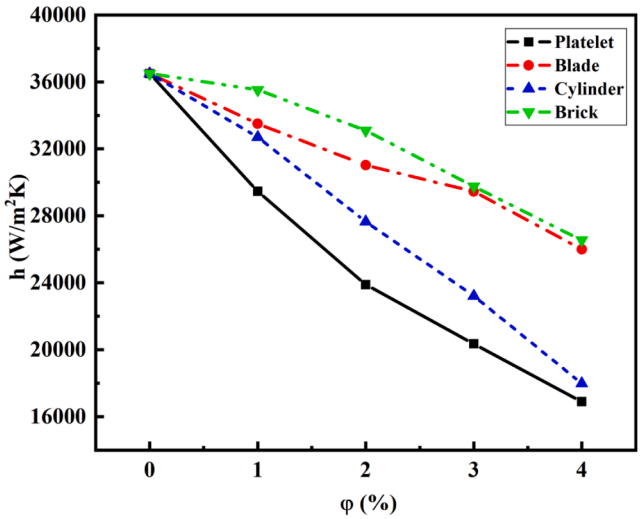

Fig. 8. FPSC h for NFs with different nanoparticle shapes, different values of φ at a FR of 0.25 kg/s in steel FPSC.

be seen that the addition of NPs causes an increase in the fluid outlet temperature. Initially, with the addition of 1% of NPs, the amount of TC_{OUT} enhancement is equal for all shapes of NPs. For φ > 1%, brick-shaped NPs have the maximum amount of TC_{OUT} and the platelet-shaped NPs have the minimum TC_{OUT}. Blade-shaped NPs lead to higher outlet temperatures than cylinders. The maximum increment in TC_{OUT} is obtained when φ = 4%, which is slightly less than 1 K.

Fig. 5 illustrates NFs TC_{OUT} with different shapes of NPs for different values of φ when the FR is 0.25 kg/s for the steel FPSC. The addition of NPs enhances the amount of fluid temperature at the output. Brick-shaped NPs are the most effective and platelet-shaped ones are the least effective NPs on the fluid outlet temperature. It can be seen that the effect of adding NPs in a steel FPSC is less than that of a copper FPSC, i.e. the temperature at the outlet is changed less. It is generally seen that using a copper FPSC can provide a fluid with a higher outlet temperature than a steel FPSC so that the copper FPSC results in a 1.86 K warmer fluid than the steel FPSC. This temperature difference for brick-shaped NPs reaches 2.15 K when φ = 4%. The higher thermal conductivity of copper results in better heat transfer than that in the steel FPSC.

Fig. 6 demonstrates water-EG outlet temperature for different FR s in copper and steel FPSCs with circular and hexagonal tubes. An increment in the FR in all cases reduces the temperature of the water-EG. An enhancement in the FR means the faster motion of fluid in the tubes, and as a result, the time for heat transfer is reduced and the fluid exits the FPSC at a lower temperature. It can be seen that the copper FPSC delivers water-EG with a higher outlet temperature than the steel FPSC. The use of a hexagonal tube in both FPSCs enhances the amount of outlet temperature compared to the circular tube. In the case of copper FPSC at a low FR, the use of hexagonal tube increases the outlet temperature by 2.67 K compared to the tube with circular cross-section. Also, this increment in steel tube is 1.75 K lower at the same FR. At high FRs, the effect of using a tube with a hexagonal cross-section is less noticeable, but it still enhances the temperature at the outlet.

Fig. 7 depicts FPSC h for NFs with different nanoparticle shapes, different values of φ at a FR of 0.25 kg/s in the copper FPSC. It can be seen that the use of NFs instead of the pure fluid reduces the amount of h, which is lower for brick-shaped NPs and higher for platelet-shaped NPs than other ones. The higher the value of φ, the lower the h. This is due to an increment in the viscosity by adding NPs and especially a reduction in the heat capacity of the fluid by adding NPs.

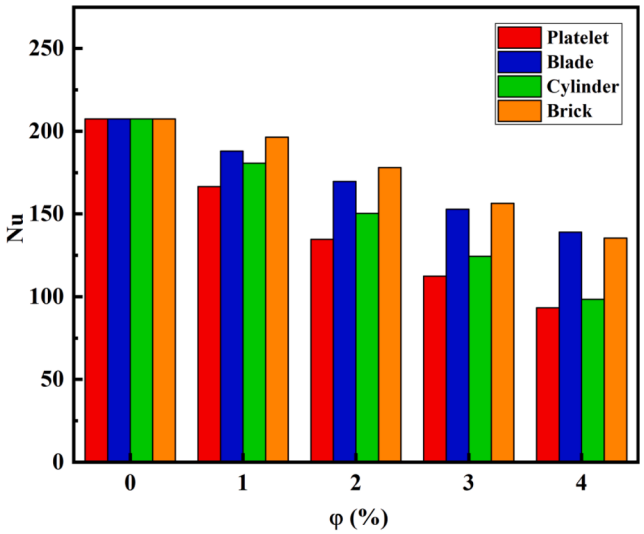

Fig. 9. Nu for different shapes and percentages of nanoparticle when the FR is 0.25 kg/s for the copper FPSC.

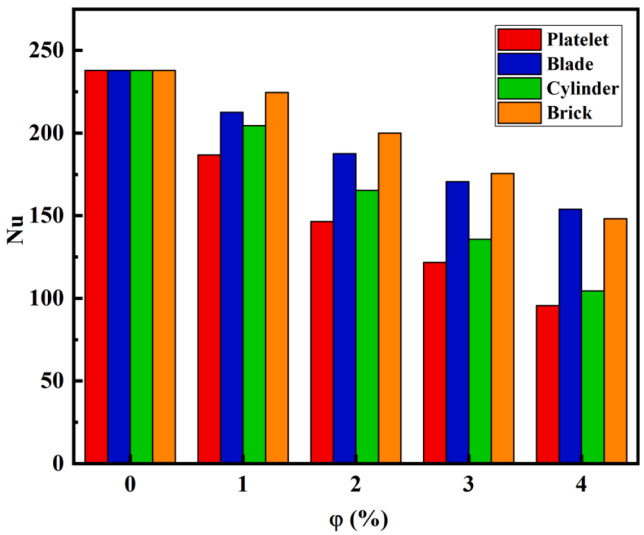

Fig. 10. Nu for different shapes and percentages of nanoparticle when the FR is 0.25 kg/s for steel FPSC.

Fig. 8 shows FPSC h for NFs with different nanoparticle shapes, different values of φ at a FR of 0.25 kg/s in steel FPSC. It is found that the h is reduced with the addition of NPs. The highest reduction is for the platelet-shaped NPs and the lowest reduction is for the brick-shaped ones. Adding 4% of the platelet-shaped NPs reduces the h by 53%. Comparing the two types of FPSC s demonstrates that the steel FPSC has a higher h than the copper one.

Fig. 9 depicts Nu for different shapes and percentages of NPs when the FR is 0.25 kg/s for the copper FPSC. It can be seen that an increment in the value of φ reduces the amount of Nu. The highest reduction and the smallest reduction correspond to brick-shaped and platelet-shaped NPs, respectively. The smallest reduction is related to $\varphi = 4\%$ for blade-shaped NPs with a 33% reduction in the Nu.

Fig. 10 shows the Nu for different shapes and percentages of NPs when the FR is 0.25 kg/s for the steel FPSC. The variations of Nu with φ for the steel FPSC are the same as those for the copper FPSC. It can be seen that the values of the Nu for the steel FPSC are more than the copper FPSC. The addition of 4% blade-shaped NPs leads to a reduction in the amount of Nu by 35%. The decreasing effect of adding NPs on Nu in steel FPSC is more than the copper FPSC.

Conclusions

In this paper, the turbulent flow of NFs in which boehmite-alumina NPs with different shapes are suspended in a mixture of water/EG in a FPSC. Also, the effect of using a hexagonal tube is compared with a circular cross-section tube. The impact of the value of φ and fluid velocity on outlet temperature, h, and Nu are studied and the following results are obtained:

1. The addition of NPs to the fluid enhances the outlet temperature of the fluid. The nanoparticle shape has the highest enhancement in outlet temperature and the platelet-shaped NPs have the lowest increment in outlet fluid temperature.
2. The use of the solar FPSC made of copper compared to the steel FPSC results in a higher output fluid temperature.
3. An enhancement in the FR reduces the amount of fluid outlet temperature.
4. Using a tube with a hexagonal cross-section enhances the outlet temperature of the fluid compared to a circular one so that the temperature in the copper and steel FPSCs enhances by 2.67 K and 1.75 K, respectively.
5. The addition of NPs reduces the amount of h and Nu in both FPSCs, which is the largest reduction for platelet-shaped NPs.
6. The h and Nu for the steel FPSC is more than the copper FPSC.

CRediT authorship contribution statement

Yacine Khetib: Conceptualization, Methodology, Formal analysis, Writing – review & editing. **Hala M. Abo-Dief:** Formal analysis, Writing – original draft, Methodology, Investigation. **Abdullah K. Alanazi:** Formal analysis, Methodology. **S. Mohammad Sajadi:** Formal analysis, Software, Data curation. **Rasool Kalbasi:** Writing – review & editing, Supervision. **Mohsen Sharifpur:** Methodology, Software, Supervision.

Declaration of Competing Interest

The authors declare that they have no known competing financial interests or personal relationships that could have appeared to influence the work reported in this paper.

Acknowledgements

This work was supported by the Taif University Researchers Supporting grant number (TURSP-2020/266) of Taif University, Taif, Saudi Arabia.

References

[1] Pordanjani AH, et al. Nanofluids: physical phenomena, applications in thermal systems and the environment effects – a critical review. J Cleaner Prod 2021: 128573.
[2] Akhtari MR, Shayegh I, Karimi N. Techno-economic assessment and optimization of a hybrid renewable earth - air heat exchanger coupled with electric boiler, hydrogen, wind and PV configurations. Renewable Energy 2020;148:839–51.
[3] Alizadeh R, Abad JMN, Ameri A, Mohebbi MR, Mehdizadeh A, Zhao D, et al. A machine learning approach to the prediction of transport and thermodynamic processes in multiphysics systems - heat transfer in a hybrid nanofluid flow in porous media. J Taiwan Inst Chem Eng 2021;124:290–306.
[4] Govone L, Torabi M, Wang L, Karimi N. Effects of nanofluid and radiative heat transfer on the double-diffusive forced convection in microreactors. J Therm Anal Calorim 2019;135(1):45–59.
[5] Habib R, Karimi N, Yadollahi B, Doranehgard MH, Li LKB. A pore-scale assessment of the dynamic response of forced convection in porous media to inlet flow modulations. Int J Heat Mass Transf 2020/06/01/ 2020.;153:119657.
[6] Habib R, Yadollahi B, Karimi N, Doranegard MH. On the unsteady forced convection in porous media subject to inlet flow disturbances-A pore-scale analysis. Int Commun Heat Mass Transfer 2020;116:104639.

[7] Saeed A, Karimi N, Hunt G, Torabi M. On the influences of surface heat release and thermal radiation upon transport in catalytic porous microreactors—A novel porous-solid interface model. Chem Eng Process – Process Intensification 2019; 143:107602.
[8] Saeed A, Karimi N, Paul MC. Analysis of the unsteady thermal response of a Li-ion battery pack to dynamic loads. Energy 2021.;231:120947.
[9] Torabi M, Karimi N, Torabi M, Peterson GP, Simonson CJ. Generation of entropy in micro thermofluidic and thermochemical energy systems-a critical review. Int J Heat Mass Transf 2020;163:120471.
[10] Li H-W, Gao Y-F, Du C-H, Hong W-P. Numerical study on swirl cooling flow, heat transfer and stress characteristics based on fluid-structure coupling method under different swirl chamber heights and Reynolds numbers. Int J Heat Mass Transf 2021;173:121228.
[11] Notton G, Motte F, Cristofari C, Canaletti J-L. Performances and numerical optimization of a novel thermal solar collector for residential building. Renew Sustain Energy Rev 2014;33:60–73.
[12] Zondag H. Flat-plate PV-Thermal collectors and systems: a review. Renew Sustain Energy Rev 2008;12(4):891–959.
[13] Sarsam WS, Kazi SN, Badarudin A. A review of studies on using nanofluids in flat-plate solar collectors. Sol Energy 2015;122:1245–65.
[14] Tagliafico LA, Scarpa F, De Rosa M. Dynamic thermal models and CFD analysis for flat-plate thermal solar collectors – a review. Renew Sustain Energy Rev 2014;30: 526–37.
[15] Muhammad MJ, Muhammad IA, Che Sidik NA, Muhammad Yazid MNAW. Thermal performance enhancement of flat-plate and evacuated tube solar collectors using nanofluid: a review. Int Commun Heat Mass Transfer 2016;76:6–15.
[16] Bayareh M, Mohammadi M. Multi-objective optimization of a triple shaft gas compressor station using Imperialist Competitive Algorithm. Appl Therm Eng 2016;109:384–400.
[17] Hussein AK. Applications of nanotechnology to improve the performance of solar collectors – recent advances and overview. Renew Sustain Energy Rev 2016;62: 767–92.
[18] Khanlari A, et al. Experimental and numerical study of the effect of integrating plus-shaped perforated baffles to solar air collector in drying application. Renewable Energy 2020;145:1677–92.
[19] Farhadi R, Taki M. The energy gain reduction due to shadow inside a flat-plate solar collector. Renewable Energy 2020;147:730–40.
[20] Choudhary S, Sachdeva A, Kumar P. Investigation of the stability of MgO nanofluid and its effect on the thermal performance of flat plate solar collector. Renewable Energy 2020.;147:1801–14.
[21] Gorji TB, Ranjbar AA. A review on optical properties and application of nanofluids in direct absorption solar collectors (DASCs). Renew Sustain Energy Rev 2017;72: 10–32.
[22] Kumar A, Prakash Om, Kaviti AK. A comprehensive review of Scheffler solar collector. Renew Sustain Energy Rev 2017;77:890–8.
[23] Sharafeldin MA, Gróf G. Experimental investigation of flat plate solar collector using CeO2-water nanofluid. Energy Convers Manage 2018;155:32–41.
[24] Han L, Lu C, Yumashev A, Bahrami D, Kalbasi R, Jahangiri M, et al. Numerical investigation of magnetic field on forced convection heat transfer and entropy generation in a microchannel with trapezoidal ribs. Eng Appl Comput Fluid Mech 2021;15:1746–60.
[25] Zhang X, Tang Y, Zhang F, Lee C-S, A Novel Aluminum–Graphite Dual-Ion Battery, vol. 6, no. 11, p. 1502588, 2016.
[26] Cheng L, Zhu Y, Band SS, Bahrami D, Kalbasi R, Karimipour A, et al. Role of gradients and vortexes on suitable location of discrete heat sources on a sinusoidal-wall microchannel. Eng Appl Comput Fluid Mech 2021;15:1176–90.
[27] Bayareh M, Mortazavi S. Effect of density ratio on the hydrodynamic interaction between two drops in simple shear flow. Iran J Sci Technol. Trans Mech Eng 2011; 35:121.
[28] Bayareh M, Dabiri S, Ardekani AM. Interaction between two drops ascending in a linearly stratified fluid. Eur J Mech-B/Fluids 2016;60:127–36.
[29] Yan S-R, Hajatzadeh Pordanjani A, Aghakhani S, Shahsavar Goldanlou A, Afrand M. Managment of natural convection of nanofluids inside a square enclosure by different nano powder shapes in presence of Fins with different shapes and magnetic field effect. Adv Powder Technol 2020;31(7):2759–77.
[30] Hu L-B, et al., MoO3 Structures Transition from Nanoflowers to Nanorods and Their Sensing Performances, 2021.
[31] Hajatzadeh Pordanjani A, Aghakhani S, Afrand M, Mahmoudi B, Mahian O, Wongwises S. An updated review on application of nanofluids in heat exchangers for saving energy. Energy Convers Manage 2019;198:111886.
[32] Tian M-W, Rostami S, Aghakhani S, Goldanlou AS, Qi C. Investigation of 2D and 3D configurations of fins and their effects on heat sink efficiency of MHD hybrid nanofluid with slip and non-slip flow. Int J Mech Sci 2020:105975.
[33] Aghakhani S, Ghasemi B, Hajatzadeh Pordanjani A, Wongwises S, Afrand M. Effect of replacing nanofluid instead of water on heat transfer in a channel with extended surfaces under a magnetic field. Int J Numer Meth Heat Fluid Flow 2019;29(4): 1249–71.
[34] Aghakhani S, Pordanjani AH, Afrand M, Sharifpur M, Meyer JP. Natural convective heat transfer and entropy generation of alumina/water nanofluid in a tilted enclosure with an elliptic constant temperature: applying magnetic field and radiation effects. Int J Mech Sci 2020/05/15/ 2020.;174:105470.
[35] Pordanjani AH, Aghakhani S. Numerical investigation of natural convection and irreversibilities between two inclined concentric cylinders in presence of uniform magnetic field and radiation. Heat Transfer Eng 2021:1–21.
[36] Borode A, Ahmed N, Olubambi P. A review of solar collectors using carbon-based nanofluids. J Cleaner Prod 2019;241:118311.
[37] Zayed ME, Zhao J, Du Y, Kabeel AE, Shalaby SM. Factors affecting the thermal performance of the flat plate solar collector using nanofluids: a review. Sol Energy 2019;182:382–96.
[38] Eidan AA, AlSahlani A, Ahmed AQ, Al-fahham M, Jalil JM. Improving the performance of heat pipe-evacuated tube solar collector experimentally by using Al2O3 and CuO/acetone nanofluids. Sol Energy 2018;173:780–8.
[39] Bellos E, Tzivanidis C. Multi-criteria evaluation of a nanofluid-based linear Fresnel solar collector. Sol Energy 2018;163:200–14.
[40] Hemmat Esfe M, Rahimi Raki H, Sarmasti Emami MR, Afrand M. Viscosity and rheological properties of antifreeze based nanofluid containing hybrid nano-powders of MWCNTs and TiO2 under different temperature conditions. Powder Technol 2019;342:808–16.
[41] Hemmat Esfe M, Rostamian H, Esfandeh S, Afrand M. Modeling and prediction of rheological behavior of Al2O3-MWCNT/5W50 hybrid nano-lubricant by artificial neural network using experimental data. Physica A 2018;510:625–34.
[42] Ranjbarzadeh R, Akhgar A, Musivand S, Afrand M. Effects of graphene oxide-silicon oxide hybrid nanomaterials on rheological behavior of water at various time durations and temperatures: Synthesis, preparation and stability. Powder Technol 2018;335:375–87.
[43] Shahsavani E, Afrand M, Kalbasi R. Using experimental data to estimate the heat transfer and pressure drop of non-Newtonian nanofluid flow through a circular tube: Applicable for use in heat exchangers. Appl Therm Eng 2018;129:1573–81.
[44] Dehaj MS, Mohiabadi MZ. Experimental investigation of heat pipe solar collector using MgO nanofluids. Sol Energy Mater Sol Cells 2019;191:91–9.
[45] Natividade PSG, de Moraes Moura G, Avallone E, Bandarra Filho EP, Gelamo RV, Gonçalves JCdSI. Experimental analysis applied to an evacuated tube solar collector equipped with parabolic concentrator using multilayer graphene-based nanofluids. Renewable Energy 2019;138:152–60.
[46] Sint NKC, Choudhury IA, Masjuki HH, Aoyama H. Theoretical analysis to determine the efficiency of a CuO-water nanofluid based-flat plate solar collector for domestic solar water heating system in Myanmar. Sol Energy 2017;155:608–19.
[47] Yan S-R, Hajatzadeh Pordanjani A, Aghakhani S, Shahsavar Goldanlou A, Afrand M. Managment of natural convection of nanofluids inside a square enclosure by different nano powder shapes in presence of Fins with different shapes and magnetic field effect. Adv Powder Technol 2020.;31(7):2759–77.
[48] Nazer-Nejad M, Saffarian MR, Behbahani-Nejad M. Investigating the possibility of using the underground tunnel for air-conditioning in Tehran. J Brazilian Soc Mech Sci Eng 2018;40:473.
[49] Menter F, "Zonal Two Equation k-w Turbulence Models For Aerodynamic Flows," in 23rd Fluid Dynamics, Plasmadynamics, and Lasers Conference, ed.
[50] Wilcox DC. Multiscale model for turbulent flows. AIAA J 1988;26:1311–20.
[51] Frei W. Which turbulence model should I choose for my CFD application? Comsol Blog 2017:1–8.
[52] Rumsey CL, Spalart PR. Turbulence model behavior in low reynolds number regions of aerodynamic flowfields. AIAA J 2009;47(4):982–93.
[53] Roy G, Gherasim I, Nadeau F, Poitras G, Nguyen CT. Heat transfer performance and hydrodynamic behavior of turbulent nanofluid radial flows. Int J Therm Sci 2012; 58:120–9.
[54] Vahidifar S, Saffarian MR, Hajidavalloo E. Introducing the theory of successful settling in order to evaluate and optimize the sedimentation tanks. Meccanica 2018;53:3477–93.
[55] Zhang L, Che D. Turbulence models for fluid flow and heat transfer between cross-corrugated plates. Numerical Heat Transfer, Part A: Applications 2011;60(5): 410–40.
[56] Menter FR. Two-equation eddy-viscosity turbulence models for engineering applications. AIAA J 1994;32:1598–605.
[57] Hellsten A, Laine S, Hellsten A, Laine S, "Extension of the k-omega-SST turbulence model for flows over rough surfaces," in 22nd Atmospheric Flight Mechanics Conference, ed.
[58] Timofeeva EV, Routbort JL, Singh D. Particle shape effects on thermophysical properties of alumina nanofluids. J Appl Phys 2009;106:014304.
[59] Bahrami D, Bayareh M, "Experimental and numerical investigation on a novel spiral micromixer with sinusoidal channel walls," Chemical Engineering & Technology, vol. n/a.
[60] Bahrami D, Bayareh M. Impacts of channel wall twisting on the mixing enhancement of a novel spiral micromixer. Chem Pap 2021:1–12.
[61] Saffarian MR, Moravej M, Doranehgard MH. Heat transfer enhancement in a flat plate solar collector with different flow path shapes using nanofluid. Renewable Energy 2020;146:2316–29.